This is an *Accepted Manuscript*, which has been through the Royal Society of Chemistry peer review process and has been accepted for publication.

Accepted Manuscripts are published online shortly after acceptance, before technical editing, formatting and proof reading. Using this free service, authors can make their results available to the community, in citable form, before we publish the edited article. We will replace this *Accepted Manuscript* with the edited and formatted *Advance Article* as soon as it is available.

You can find more information about *Accepted Manuscripts* in the **Information for Authors**.

Please note that technical editing may introduce minor changes to the text and/or graphics, which may alter content. The journal's standard **Terms & Conditions** and the **Ethical guidelines** still apply. In no event shall the Royal Society of Chemistry be held responsible for any errors or omissions in this *Accepted Manuscript* or any consequences arising from the use of any information it contains.

Structure Evolution of NiAu Nanoparticles under Ambient Conditions Revealed Directly by Atom-resolved Imaging Combined with DFT Simulation

Xia Xiang,[†] Jinlan Nie,[†] Kai Sun,[‡] Li Zhang,[†] Wei Liu,[*,†,‡] Johannes Schwank,[§] Shifa Wang,[†] Mian
5 **Zhong[†], Fei Gao[∥] and Xiaotao Zu[*,†]**

Abstract: For noble-transition bimetallic catalysts, the structure stability evaluates as significant as the well-studied catalytic efficiency in economic point of view. The structure evolution and corresponding dynamics of NiAu bimetallic
10 nanoparticles under ambient conditions are investigated using *in situ Cs*-corrected STEM and DFT calculations. In oxidization, Au component promotes dissociation of oxygen and initiates Ni oxidization, which simultaneously drives the migration of Au atoms yielding multi-shell structures, denoted by Ni@Au@NiO. The subsequent hydrogen reduction induces surface reconstruction forming fcc-NiAu clusters. After cycles of catalyzing CO oxidation, inverse Au segregation and Ni recrystallization occur ascribed to exothermic excitations. The results of this study can help to
15 understand the evolution behaviors of the bimetallic nanoparticles under ambient conditions as well as to optimize the structure design of bimetallic catalysts.

Introduction

The distinct synergy of two components that can introduce
20 superior catalytic properties has made noble-transition bimetallic materials attract increasing research efforts during the past few years.[1-3] Evaluation of such nanostructured catalyst falls into two aspects, catalytic efficiency and activity stability. For the former aspect, previous work has succeed in achieving continuous
25 promotion of catalytic efficiency through designing the surface configuration for more active sites[4-8], utilizing noble component in form of single atom[9-11], reducing coordination number of surface atom via clusters assembly approach[12, 13]. For the catalytic stability, however, less attention has been paid as known
30 as so far even it plays a role as important as the efficiency in potential applications of the catalysts[14-16]. Especially less concern has been paid for their structure stability in ambient atmospheres of realistic perspective, including surface oxidization decontamination and subsequent hydrogen reduction for catalyst
35 reactivation as well as running catalytic cycles. Known that the catalytic stability of a bimetal sensitively relies on the surface conditions that influence the binding energy of surface atoms, including component configurations, structural defects, and surface oxidization states.[17-20] These surface parameters can be
40 changed ascribed to the competition of ordering- and clustering-type in the alloy system (e.g. the competition between $L1_2$ and $Z1$ phases in fcc Au-Ni system), where the phase transfer occurs under thermal excitation at level of tens of meV.[21] Such energy value can be easily satisfied in a typical catalytic reaction
45 step.[2, 9, 22] Furthermore, previous works has proved the change in catalyst composition can also modulate the catalyst activity and thus control the reaction behavior and morphologies of final products.[23]

Disclosing the delicate evolution behaviors of bimetallic
50 nanostructure in typical atmospheres through atom-resolved in-situ observation has become a crucial issue pursued by researchers before it comes to practical application. The advantages of spherical aberration (C_s) correctors equipped on scanning transmission electron microscope (STEM) make it a
55 powerful tool for characterizing atomic structures of crystals with multi-components, especially for the multi-metallic ones benefiting for their large atomic number difference and outstanding irradiation resistance.[24-27] Further combined with environmental reaction facilities of either E-cell holder[28-30] or
60 ETEM[22, 31], it enables direct observation of an individual heterogeneous nanostructure at atomic level, from which the delicate atmosphere-related structure evolution can be registered with a specific nanoparticle.[32-35] However, several critical aspects have to be carefully considered before give conclusions through
65 these *in situ* environmental observations: i) the knock-on sputtering effect in microscope as well as the electron stimulated desorption of gas molecules; ii) the thermal desorption of molecules induced by electron irradiation; iii) the environmental pressure is always limited far below ambient pressure to ensure
70 efficient spatial resolution (typically lower than 20 mbar for resolution better than 0.2 nm).[36] These factors can change the reaction conditions, which have possibilities of blocking the achieving of intrinsic information of catalytic reactions under ambient conditions.

75 Here, we report an *in situ* study on atmosphere-related atomic structure evolutions of NiAu nanoparticles under ambient pressure. Fantastic structure evolution has been observed of several selected NiAu bimetallic nanoparticles during oxidation, reduction as well as a catalytic cycle, including the components
80 diffusion driven by oxidization, surface amorphization induced by reduction and the inverse segregation and recrystallization in catalytic reaction. Density functional theory (DFT) simulations reveal that the Au atoms promote the Ni oxidization by driving the dissociation of nearby oxygen molecule, and simultaneously
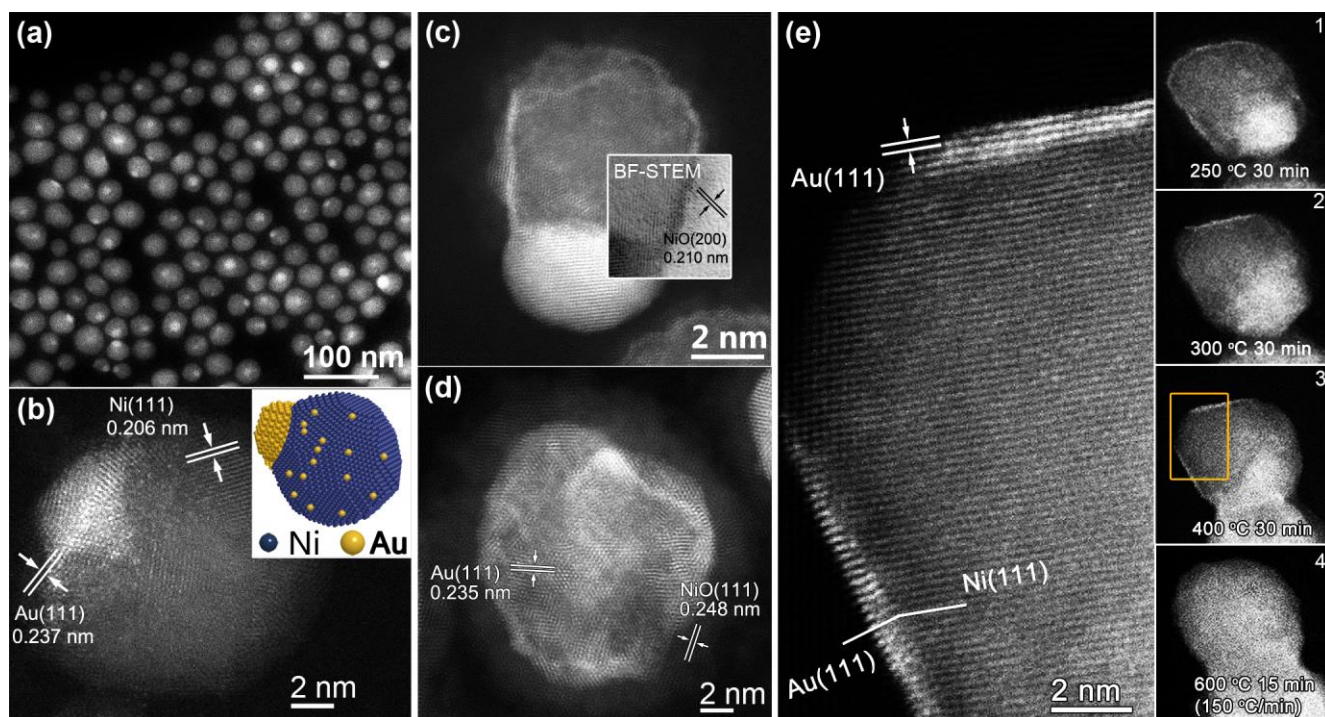
Figure 1. HADDF images of NiAu nanoparticles in conditions of: as-synthesized (a~b), oxidized (c~d) and vacuum annealed (e), respectively. (a) low magnified overview of as prepared samples; (b) an individual NiAu particle with spindle-like morphology, the inset is the corresponding schematic model; (c) a typical NiAu particle after the exposure in air for 85 days at room temperature, the inset is the simultaneously collected STEM-BF image giving clear lattice fringes of a NiO shell; (d) a NiAu particle annealed at 350 ^{o}C for 8 hours in air, forming an ideal Ni@Au@NiO multilayer structure; (e) *in situ* observation of NiAu reconstruction in vacuum annealing through four stages (insets of 1 to 4) as the temperature increases, the atom-resolved HADDF image was taken from marked area of inset 3.

diffuse to form the Au shell on the residual Ni core. During reduction, the as-reduced Ni atoms will incorporate into the Au layer forming amorphous alloy surface composed of NiAu clusters in fcc configuration. During the catalytic cycle, the particle surface recrystallizes and Au atoms turn to segregate onto the surface under the exothermal excitations of the catalytic reaction.

Results and discussions

Taking the advantages of high resolution HAADF imaging, the atomic structures of the NiAu nanospindles in different conditions are briefly demonstrated in Fig. 1 (Au atoms show much brighter contrast). For the original NiAu particles (Fig. 1a~1b), most Au component separates at one side of the Ni matrix leaving a small amount of single Au atoms dispersed in the Ni matrix and these monodispersed atoms are more active and with high mobility in either oxidizing atmosphere or vacuum annealing but initiate rather different structure reconstruction behaviors. When these bimetallic nanoparticles were exposed in air at either room (~20 ^{o}C) or promoted temperatures (350 ^{o}C), oxidization induces the formation of multilayer structures with the Au component dispersing into the shells on the residual Ni cores and NiO layer as the outermost shells, i.e., forming Ni@Au@NiO multilayer structures as shown in Fig. 1d. Figure 1c shows an obvious snapshot of such a reconstruction process where the Au component has partially dispersed along the Ni matrix. For the case of *in-situ* annealed in vacuum (Fig. 1e) which provides detailed understanding on the thermal stability of

the NiAu nanostructures, the nanostructures evolve through four distinct steps with the increase of temperature: (i) polyhedron recrystallization of Ni matrix (inset 1); (ii) facets-selected segregation of monodispersed Au component (inset 2); (iii) single crystallization of Ni matrix (Fig. 1e and inset 3); (iv) wrapping diffusion of Au component (inset 4). The lattice spacings from the fcc structure were labeled. The monodispersed Au atoms show higher mobility at low temperature (400 ^{o}C), while the wrapping diffusion of main Au component at high temperature (600 ^{o}C or even higher) can be ascribed to the lattice stress between two components and the significantly reduced migration barrier in a quasi-molten state (more details about thermal annealing induced structure changes in air and vacuum can be found in Fig. S1 and Fig. S2, respectively). Herein it should be noted that the diffusion of Au atoms in the oxidizing atmosphere (starting from room temperature) is much easier than that in vacuum (starting above 400 ^{o}C), which reveals that the oxidation environment should account for such difference. Moreover, since the Au and Ni components separate on two sides in the original NiAu structure and the Ni phase can be oxidized especially at promoted temperature, a Au-separated Ni@NiO structure should be expected in the oxidation condition rather than the Ni@Au@NiO multilayer structure.

The question comes what drives Au atoms to migrate? To answer such a question, we have carried out extensive theoretical investigation based on DFT. According to above microscopy results, the epitaxial dispersion of Au component on Ni(111) surface of inside nickel matrix dominates the configurations of the two phases, which coincides with the experience from
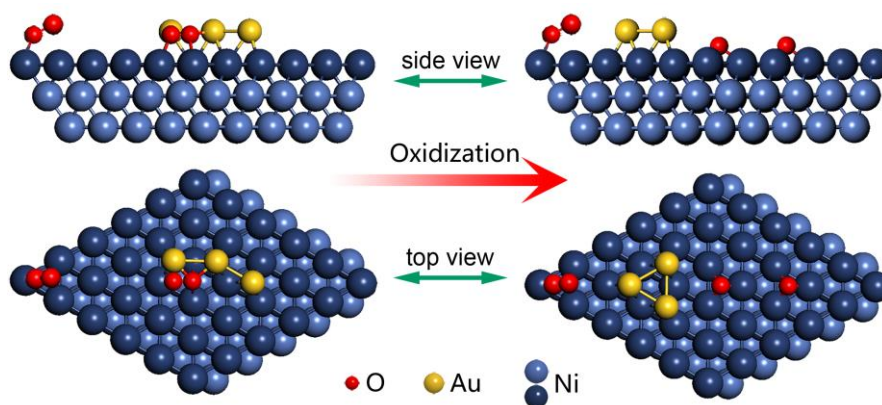
Figure 2. Optimized structures of the Au assisted Ni oxidization process (side view and top view). The left two images show the configurations of oxygen (red) absorption near/away from the Au (yellow) sites on the Ni(111) surface (light/dark blue); the right two images illustrate the configurations of Au-induced dissociation of oxygen molecule, Ni oxidization, as well as the dispersion of Au atoms. The Au atoms have been intentionally shrunk to give better illustration of structure detail.

previous reports.[8, 37] Therefore we built a slab model with three adjacent Au atoms on a five-layer Ni(111) support (nine Ni atoms per layer). Considering the ferromagnetism of Ni, the spin polarization was also considered throughout the calculations. Figure 2 provides schematic illustration of the possible configurations during oxidization process. The calculations turned out that two of the three adjacent Au atoms prefer to occupy the three-fold hcp sites (in a "ABAB" stacking sequence with Ni support) while another on the fcc site (in a "ABCABC" stacking sequence with Ni support).

Based on this optimized Ni(111)(3×3):3Au structure, the adsorption behavior of oxygen on the surface of the model structure has been investigated. In order to compare the adsorption behavior of oxygen nearby or being away from the Au atoms, we accordingly considered two situations, i.e. one situation with O_2 close to one of the Au atoms (the lateral distance is ~1.4 Å), another one with the lateral distance of about 3.3 Å. The calculations show that the O_2 molecule close to the Au atoms dissociates and the adjacent three Au atoms migrate on the Ni(111) surface upon structural optimization for the first situation, resulting in compact arrangement as shown in Fig. 2 (Au atoms sit on three adjacent hcp hollow sites). Differently, for the second situation in which the oxygen molecule is away from the Au atoms, no apparent change of the atom arrangement has been observed, except for the slight elongation of the O-O bond from 1.235 Å (for the isolated O_2) to 1.45 Å. The energetics analysis showed that the dissociative adsorption of oxygen in the first situation is up to 1.884eV, which is more stable than the molecular adsorption in the second situation, revealing the remarkable promotion of Ni oxidization near the Au atoms. These results indicate that: (1) the oxygen nearby Au atom tends to dissociate, which subsequently promotes the oxidation of Ni substrate; (2) the dissociation of oxygen drives the migration of Au atoms in turn, and they tend to occupy the adjacent three-fold hollow sites, based on which an ideal Au shell is predictable. The migration of Au atoms into compact arrangement driven by oxygen dissociation is thought to account for the experimentally observed crystalline structures of Au component (Fig. 1c and 1d). In addition, considering the lattice matching stresses, NiO phase (with largest lattice spacings in the three phases) is driven to the outermost layer during mass transportation leaving the Au diffusion layer in the middle and the residual Ni (smallest lattice spacings) as the core. A short movie (Au Assisted Ni Oxidization_movie.avi) has been made to show the above dynamics, which accounts for the experimental formation of Ni@Au@NiO multilayer structure.

The evolution behaviors of NiAu nanostructure in practical catalytic cycles, including the decontamination process and subsequent hydrogen reduction as well as the catalytic oxidation of CO are studied here. Generally, the overview of element distribution shown in the pseudo-colored insets from marked area of Fig.3a~3c manifests similar contrast change, revealing the identity of reconstruction manners of the three particles. Specially, after the insufficient oxidization in air for 30 min, the bimetallic particle maintains the separation of Au and Ni components but wrapped outside by a NiO layer (~1nm in thickness) as shown by Fig. 3a. Clear lattice fringes are visible for all three phases and the diffusion of Au component is not obvious.

When reduced in hydrogen at 300 °C for 30 min, obvious amorphization on the particle surface was observed (Fig.3b). The diffusion trend of Au component is remarkable during the reduction noting that the brighter Au tip has nearly disappeared (the area marked by green dashed ellipse of Fig. 3d~3e). Besides, the contrast of Au atomic columns in the HAADF image (Fig. 3e) is weak, discrete and with fuzzy edges compared with their appearance of Fig. 3d, especially at the edges of particles where an amorphous alloy layer has been substituted for NiO layer induced by hydrogen reduction. All these features evidence that the reduced Ni atoms from the NiO layer has migrated into the Au layer forming an amorphous mixture layer composed of clusters The STEM-BF images (Fig. S3) simultaneously acquired with those in Fig. 3 provide more intuitive demonstration on the crystallinity change. Another effect of hydrogen reduction is to arouse the partial combination of adjacent two particles and the contact point becomes rich with the Au component as shown in the areas marked by yellow dashed ellipse in Fig. 3e. Such behavior is much similar with that during the vacuum annealing aforesaid, which can also be contributed to the spontaneously minimization of surface energy.
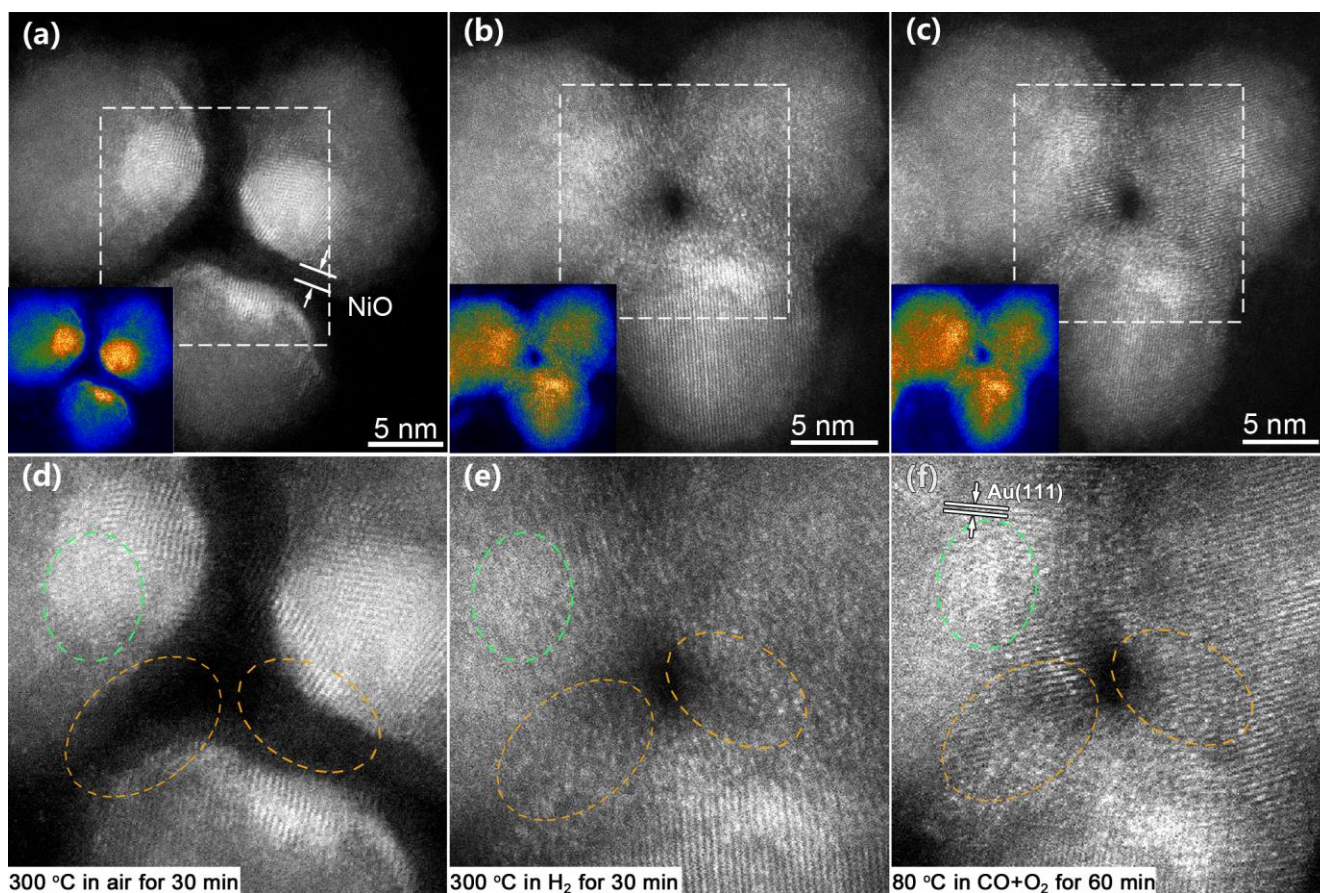
Figure 3. *In situ* observed NiAu reconstruction in a series of catalytic reactions. (a~c) HAADF images of the same three-particle region after air oxidization (300 ^{o}C in air for 30 min), hydrogen reduction (300 ^{o}C in H$_2$ for 30 min) and catalytic reaction (80 ^{o}C in CO+O$_2$ for 60 min), respectively. (d~f) the corresponding high magnified HAADF images from the marked regions of image (a~c), respectively.

After the focused NiAu nanostructures having been subjected to the catalyzing oxidation of CO at 80 ^{o}C for 1h, their atomic structures were further changed as shown in Fig. 3c and 3f. It is fantastic to discover that the Au component demonstrates a segregation trend to gather on the surface as shown by the inset of Fig. 3c. There even forms stable crystal lattice in some areas (circled by green line in Fig. 3f), which is also verified by STEM-BF imaging (Fig. 3S). Meanwhile, an obvious crystallinity promotion on NiAu surface can be noted with sharp contrast of Au columns embedded in Ni fringes.

As having been observed, the oxidation process would drive both the Ni and Au atoms to migrate. It is intriguing to find that such reaction-driving migration of surface atoms also apply to the situation of hydrogen reduction. On the contrary, the catalytic oxidation process enables the inverse reconstruction of NiAu nanostructure, including the surface segregation of Au component as well as the recrystallization of Ni matrix. These evidences bring questions on how the surface atoms will rearrange in subsequence of the collapse of NiO layer due to the absence of O atoms during reduction, and what are the dynamics to coordinate the Au migration, Ni/NiO phase transition and surface recrystallization? To understand the reconstruction dynamic of the Ni/Au/NiO structure at atomic level, we also adapted DFT simulations on the basis of model structures previously optimized shown in Fig. 2. To simplify the computation, we left out the reaction details between hydrogen and apex O atom on the crystal

NiO surface but started the DFT optimization after the desorption of water molecules. The configuration of as-reduced Ni atoms adapting on the Au layer was considered in the representative slab model as shown in Fig. 4. Six Au atoms on Ni(111) (3×3) surface were considered, representing the diffused Au shell supported on the residual Ni core. Four Ni atoms initially on the Ni(111) lattice site were adopted to model the Ni atoms reduced from NiO layer. The results show that the outermost layer of as-reduced Ni atoms has completely rearranged upon structural optimization with the Ni atoms partially incorporating into the Au layer. While the rest of Ni atoms (indicated by black arrow in left top view of Fig. 4) that are initially closer to the Au atoms (i.e. with less space beneath) are found to migrate on the Au surface toward the adjacent lattice site (indicated by white arrows in left top view of Fig. 4). The rumpling of the Au layers is observed as well, which may be attributed to the contraction of Au layer driven by the neighboring accumulated Ni atoms and the stress of lattice expansion. In the case of reduction at promoted temperature (300 ^{o}C), such distortion of Au lattices induced by the Ni incorporation could be more drastic and even completely confuses the original crystallinity of Au layer. This mechanism accounts for the surface amorphization of as-reduced NiAu particles. Moreover, according to our simulations, a common structure of Au and as-reduced Ni atoms follows a fcc configuration (occupy the A, B, and C sites, respectively) as shown in the right top view of Fig. 4. The unit size of this
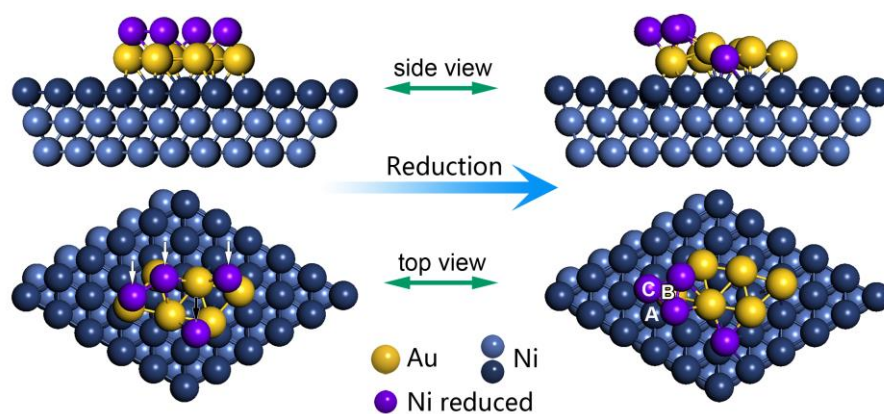
Figure 4. Optimized structures of the Ni(111)/Au/NiO multilayer slab before (left two images) and after (right two images) the surface reconstruction driven by hydrogen reduction. The left two images show the configuration of as-reduced Ni atoms (purple) adapting on the Au layer (yellow) that is supported on the Ni(111) surface (light/dark blue); the right two images illustrate the configuration reconstructed from the original structure (left two images) through DFT optimization.

structure is estimated to be 0.3 nm, which is actually coincident with the mean diameter of NiAu clusters measured from the experimental results (Fig. S4). This discovery further supports the rationality of our simulations based on the experimental data.

Considering the structure reconstruction behavior of the NiAu nanoparticles in the catalytic reaction (herein the oxidization of CO), a catalytic cycle can be divided into several steps that have been well studied in previous works,[2, 9, 37] including absorption of CO and O_2 molecules, dissociation of O_2 and simultaneous Ni oxidization, transfer of oxygen atom from NiO to CO (also known as CO oxidation), and desorption of CO_2 molecules. From the energy point of view, remarkable surface energy fluctuations appear at two steps in each catalytic cycle. One step is the O_2 absorption and Ni oxidization where the absorption energy reduces by ~1.0 eV,[2, 8, 9] our results of both experiments and calculations has attested that the dissociation of the oxygen can drive the dispersion of the Au atoms along the Ni(111) surface. Another step is the CO oxidation coupled with breaking of Ni-O bond where the activation barrier could be as small as ~0.46 eV,[8] whereas the CO oxidation reaction is exothermic by up to 2.0 eV[2, 9] and such abundant energy shall drive surface reconstruction (noting in our vacuum annealing that the equivalent energy for Au diffusion is only at level of 0.1 eV). Moreover, Reichert H. and co-workers reported the competition of ordering- and clustering-type in the NiAu alloy system, where the Au_3Ni of fcc phase (also observed in our results) can transfer into Au_3Ni_2 phase under thermal excitation at level of tens of meV.[21] This may provide interpretations on the observed Au segregation and Ni recrystallization on the surface noting that the fcc configuration of Ni and Au for the outermost two layers could be reconstructed under the exothermic excitations.

Experimental details

The NiAu nanospindles were synthesized in a mild chemical solution system using oleylamine as both solvent and reductant as reported in our former work.[38] Structure characterizations were performed on the same batch of sample to ensure the comparability of structure evolution behaviors in different atmospheres. A JEOL JEM 2100F microscope with a STEM probe corrector (CEOS GmbH probe corrector) was used in STEM mode that gives a spatial resolution of ~0.1nm. Both STEM bright-field (STEM-BF) and high-angle annular dark-field imaging (HAADF) images were collected simultaneously to achieve comprehensive information of the same hybrid nanostructure. The lens settings define the collect angle for HAADF imaging to be around 50 mrad, which enables the direct observation of atoms with different atomic numbers. A catalytic cycle of CO oxidation as well as the preliminary surface treatment (including decontamination via oxidation and hydrogen reduction) was processed in the cell of Bruker Tensor 27 spectrometer. For the pre-oxidation process, an air flow of 30 ml/min was introduced into the cell at temperature of 300 °C for 30 min to eliminate the possible organic residual on the surface of NiAu nanospindle. Then a gas mixture of 2% H_2 (99.999%) and 98% N_2 (99.999% pure) was at flow rate of 30 ml/min was inlet for another 30 min at 300 °C remove the oxidization state at sample surface. In the following catalytic cycle, a gas mixture of 1% CO (99.5% pure, Al tank) and 99% N_2 (pure) at a flow rate of 30 ml/min was inlet for 1h at each temperature for CO adsorption. Then the cell was pumped to 1×10^{-5} mbars to remove the gaseous CO species. For CO oxidation, a gas mixture of 1% CO, 1% O_2 (99.999% pure) and 98% N_2 at a total flow rate of 30 ml/min was inlet for 1h at 80 °C (a standard temperature for catalytic oxidization of CO). After each of above procedures, the sample was first cooled to room temperature under pure N_2 and was then transferred into the microscope immediately (less than 15 min) so as to reduce any additional structure change of the sample.

Conclusions

In conclusions, the atmosphere related structure evolution of NiAu nanoparticles are studied by combined quasi *in-situ* HAADF imaging at atomic scale and DFT calculations. In the oxidation atmosphere, the oxygen molecules near the Au cluster tend to dissociate and bond with Ni atoms initiating the occurrence of Ni oxidation. Simultaneously, the approaching and dissociation of O_2 drive the diffusion of Au atoms along the Ni(111) surface resulting in the formation of the Ni@Au@NiO multi-shell structures with the assist by lattice matching stresses. During hydrogen reduction, the drastic removal of O atoms leads

to the collapse of the NiO layer followed by the amorphous reconstruction of Ni, Au atoms with partial Ni atoms incorporated into the Au layer and the rest diffuse to the Au surface forming alloy clusters with fcc configurations. Differently, the oxidation process enables the inverse reconstruction of NiAu nanostructure, including the surface segregation of Au component as well as the recrystallization of Ni matrix, which can be attributed to the exothermic excitations of catalytic reaction. The knowledge on the distinct reconstruction behaviors of NiAu bimetallic system in diverse atmospheres provides guideline in structural design and optimization of performance of bimetallic catalysts.

Acknowledgements

Notes and references

* *Address correspondence to: weiliu@uestc.edu.cn; xtzu@uestc.edu.cn*
† *School of Physical Electronics, University of Electronic Science and Technology of China, Chengdu 610054, China*
‡ *Department of Materials Science and Engineering, University of Michigan, Ann Arbor, MI 48109, USA*
§ *Department of Chemical Engineering, University of Michigan, Ann Arbor, MI 48109, USA*
‖ *Pacific Northwest National Laboratory, P.O. Box 999, Richland, WA 99352, USA*

Electronic Supplementary Information (ESI) available: [BF/DF-STEM images of NiAu NPs in vacuum, O_2, H_2, CO oxidization; reconstruction movie in oxidization based on DFT simulation. (Figs S1-S4) is available in the Supplementary Information.] See DOI: 10.1039/b000000x

1. S. H. Sun, C. B. Murray, D. Weller, L. Folks and A. Moser, *Science*, 2000, **287**, 1989-1992.
2. I. X. Green, W. J. Tang, M. Neurock and J. T. Yates, *Science*, 2011, **333**, 736-739.
3. C. Antoniak, M. E. Gruner, M. Spasova, A. V. Trunova, F. M. Roemer, A. Warland, B. Krumme, K. Fauth, S. Sun, P. Entel, M. Farle and H. Wende, *Nat. Commun.*, 2011, **2**, 528.
4. W. Zhou, J. B. Wu and H. Yang, *Nano Lett.*, 2013, **13**, 2870-2874.
5. C. Wang, H. Daimon and S. H. Sun, *Nano Lett.*, 2009, **9**, 1493-1496.
6. Y. Q. Zheng, J. Tao, H. Y. Liu, J. Zeng, T. Yu, Y. Y. Ma, C. Moran, L. J. Wu, Y. M. Zhu, J. Y. Liu and Y. N. Xia, *Small*, 2011, **7**, 2307-2312.
7. X. Y. Liu, A. Q. Wang, T. Zhang and C. Y. Mou, *Nano Today*, 2013, **8**, 403-416.
8. J. Knudsen, L. R. Merte, G. W. Peng, R. T. Vang, A. Resta, E. Laegsgaard, J. N. Andersen, M. Mavrikakis and F. Besenbacher, *Acs Nano*, 2010, **4**, 4380-4387.
9. B. T. Qiao, A. Q. Wang, X. F. Yang, L. F. Allard, Z. Jiang, Y. T. Cui, J. Y. Liu, J. Li and T. Zhang, *Nat. Chem.*, 2011, **3**, 634-641.
10. X. F. Yang, A. Q. Wang, B. T. Qiao, J. Li, J. Y. Liu and T. Zhang, *Accounts Chem. Res.*, 2013, **46**, 1740-1748.
11. J. Zhang and A. N. Alexandrova, *J. Phys. Chem. Lett.*, 2013, **4**, 2250-2255.
12. J. L. Liu, W. Liu, Q. Sun, S. G. Wang, K. Sun, J. Schwank and R. M. Wang, *Chem. Commun.*, 2014, **50**, 1804-1807.
13. H. J. Zhang, T. Watanabe, M. Okumura, M. Haruta and N. Toshima, *J. Catal.*, 2013, **305**, 7-18.
14. P. L. Hansen, J. B. Wagner, S. Helveg, J. R. Rostrup-Nielsen, B. S. Clausen and H. Topsoe, *Science*, 2002, **295**, 2053-2055.
15. R. M. Wang, O. Dmitrieva, M. Farle, G. Dumpich, H. Q. Ye, H. Poppa, R. Kilaas and C. Kisielowski, *Phys. Rev. Lett.*, 2008, **100**, 017205.
16. R. M. Wang, H. Z. Zhang, M. Farle and C. Kisielowski, *Nanoscale*, 2009, **1**, 276-279.
17. G. Kyriakou, M. B. Boucher, A. D. Jewell, E. A. Lewis, T. J. Lawton, A. E. Baber, H. L. Tierney, M. Flytzani-Stephanopoulos and E. C. H. Sykes, *Science*, 2012, **335**, 1209-1212.
18. E. Nikolla, J. Schwank and S. Linic, *J. Am. Chem. Soc.*, 2009, **131**, 2747-2754.
19. J. Suntivich, Z. C. Xu, C. E. Carlton, J. Kim, B. H. Han, S. W. Lee, N. Bonnet, N. Marzari, L. F. Allard, H. A. Gasteiger, K. Hamad-Schifferli and Y. Shao-Horn, *J. Am. Chem. Soc.*, 2013, **135**, 7985-7991.
20. P. S. West, R. L. Johnston, G. Barcaro and A. Fortunelli, *Eur. Phys. J. D*, 2013, **67**, 165.
21. H. Reichert, A. Schops, I. B. Ramsteiner, V. N. Bugaev, O. Shchyglo, A. Udyansky, H. Dosch, M. Asta, R. Drautz and V. Honkimaki, *Phys. Rev. Lett.*, 2005, **95**, 235703.
22. Y. Kuwauchi, S. Takeda, H. Yoshida, K. Sun, M. Haruta and H. Kohno, *Nano Lett.*, 2013, **13**, 3073-3077.
23. X. Z. Liao, A. Serquis, Q. X. Jia, D. E. Peterson, Y. T. Zhu and H. F. Xu, Appl. Phys. Lett., 2003, **82**, 2694-2696.
24. M. Haider, S. Uhlemann, E. Schwan, H. Rose, B. Kabius and K. Urban, *Nature*, 1998, **392**, 768-769.
25. A. Mayoral, S. Mejia-Rosales, M. M. Mariscal, E. Perez-Tijerina and M. Jose-Yacaman, *Nanoscale*, 2010, **2**, 2647-2651.
26. U. Falke, A. Bleloch, M. Falke and S. Teichert, *Phys. Rev. Lett.*, 2004, **92**, 116103.
27. Y. K. Takashi Yamazaki, Mineharu Tsukadaa and Yuji Kataokaa, *Ultramicroscopy*, 2010, **110**, 1161-1165.
28. H. M. Zheng, R. K. Smith, Y. W. Jun, C. Kisielowski, U. Dahmen and A. P. Alivisatos, *Science*, 2009, **324**, 1309-1312.
29. J. F. Creemer, S. Helveg, G. H. Hoveling, S. Ullmann, A. M. Molenbroek, P. M. Sarro and H. W. Zandbergen, *Ultramicroscopy*, 2008, **108**, 993-998.
30. T. Yaguchi, M. Suzuki, A. Watabe, Y. Nagakubo, K. Ueda and T. Kamino, *J. Electron Microsc.*, 2011, **60**, 217-225.
31. P. L. Gai, *Top. Catal.*, 2002, **21**, 161-173.
32. Y. Ding, F. R. Fan, Z. Q. Tian and Z. L. Wang, *J. Am. Chem. Soc.*, 2010, **132**, 12480-12486.
33. H. Yoshida, Y. Kuwauchi, J. R. Jinschek, K. J. Sun, S. Tanaka, M. Kohyama, S. Shimada, M. Haruta and S. Takeda, *Science*, 2012, **335**, 317-319.
34. V. C. Holmberg, K. A. Collier and B. A. Korgel, *Nano Lett.*, 2011, **11**, 3803-3808.
35. M. M. Mariscal, A. Mayoral, J. A. Olmos-Asar, C. Magen, S. Mejia-Rosales, E. Perez-Tijerina and M. Jose-Yacaman, *Nanoscale*, 2011, **3**, 5013-5019.
36. A. N. Bright, K. Yoshida and N. Tanaka, *Ultramicroscopy*, 2013, **124**, 46-51.
37. S. A. Tenney, W. He, C. C. Roberts, J. S. Ratliff, S. I. Shah, G. S. Shafai, V. Turkowski, T. S. Rahman and D. A. Chen, *J. Phys. Chem. C*, 2011, **115**, 11112-11123.
38. W. Liu, K. Sun and R. M. Wang, *Nanoscale*, 2013, **5**, 5067.